SEMARAK ILMU PUBLISHING

CFD Letters

Journal homepage:
https://semarakilmu.com.my/journals/index.php/CFD_Letters/index
ISSN: 2180-1363

Numerical Investigation of Trim and Sinkage Effect on Resistance of a Semi-planing Monohull

Ahmad Nasirudin[1], Sutiyo[2], Dominic Hudson[3], I Ketut Aria Pria Utama[1,*]

[1] Department of Naval Architecture, Faculty of Marine Technology, Institut Teknologi Sepuluh Nopember, Surabaya 60111, Indonesia
[2] Department of Naval Architecture, Faculty of Engineering and Marine Sciences, Universitas Hang Tuah, Surabaya 60111, Indonesia
[2] Department of Civil, Maritime and Environmental Engineering, Faculty of Engineering and Physical Sciences, University of Southampton, United Kingdom

ARTICLE INFO

Article history:
Received 7 November 2023
Received in revised form 10 December 2023
Accepted 15 January 2024
Available online 31 August 2024

Keywords:
Trim; sinkage; resistance; semi-planing monohull; computational fluid dynamics

ABSTRACT

Trim and sinkage of a ship have a significant impact on its resistance, particularly in the case of semi-planing vessels, where the degree of trim and sinkage can vary considerably depending on the ship's speed. In this study, a computational fluid dynamics analysis was carried out to investigate trim and sinkage effect on a semi-planing monohull ship model at six different speeds, with Froude numbers (Fr) ranging from 0.2 to 0.7. The study investigates a ship model resistance with completely no trim and sinkage (fixed condition) and a ship with natural motion with trim and sinkage (free condition). The findings show that a total resistance of free condition is higher than the fixed condition, with the largest difference being 68.4% occurring at Fr 0.6. From the investigation shows that the dominant factor influencing the resistance is the residuary resistance, while the friction resistance is not significantly affected by trim and sinkage conditions.

1. Introduction

The condition of trim and sinkage undoubtedly affects the resistance of a ship. Trim refers to the longitudinal inclination of a ship, while sinkage refers to the vertical submersion of the ship's hull. These two factors are closely related and can significantly impact the resistance experienced by a ship as it moves through the water.

The trim and sinkage conditions of ships are affected by different factors such as hull type and shape, speed, and loading conditions. For displacement hulls where they operate at low speed, trim and sinkage are highly influenced by its loading condition. Meanwhile For semi-planing and planning hulls where they operated at higher speed, trim and sinkage is affected besides being influenced by loading conditions, they are also influenced by their speed [1].

Trim and sinkage can sometimes be advantageous and sometimes disadvantageous. Several studies have been conducted to control the trim and sinkage conditions of a ship during operation by adding appendages such as stern flap, stern wedge, or foil with the aim of obtaining minimum

* *Corresponding author.*
E-mail address: kutama@na.its.ac.id (I Ketut Aria Pria Utama)

https://doi.org/10.37934/cfdl.17.1.4659

resistance [2-10]. Salas *et al.,* [2] investigated the effect of stern flap on resistance of a semi-displacement hull. The results showed that stern flaps can significantly reduce resistance and increase maximum attainable speed. Ghassemi *et al.,* [6] investigated the effect of a stern wedge on the hydrodynamic performance of a chine-planing hull. The results showed that increasing the length of the stern wedge reduces drag and trim of the hull. Suastika *et al.,* [10] investigated the effects of applying a stern foil on ship resistance. The study was conducted using CFD and verified with model test data. A 40-meter Orela crew boat with a target top speed of 28 knots was considered. The results show that at relatively low speeds, the application of a stern foil increases ship resistance by up to 13.9%, while at relatively high speeds, it decreases resistance by up to 10.0%. The Froude number also plays a role in ship resistance, with the maximum value occurring at approximately 0.5. These findings contribute to the existing literature on the application of stern foil as a resistance reduction device.

The above review shows that low resistance can be obtained by controlling the trim and sinkage at the appropriate condition. Based on those results, an idea to investigate a ship resistance with completely no trim and sinkage (fixed condition) and a ship with natural motion with trim and sinkage (free condition) is conducted. A numerical investigation by using Computational Fluid Dynamics (CFD) is used and a typical semi-planing monohull is chosen in this study.

2. Methodology

2.1 Model Geometry and Investigation Configurations

The study employed a model of semi-planing monohull with about 2 meters length [11]. The detail particulars and its hullform are shown in Table 1 and Figure 1.

Table 1
Semi-planing model particulars

Particulars	Value
LOA	2.00 m
LWL	1.87 m
B	0.36 m
H	0.32 m
T	0.12 m
Cb	0.46
Displacement (□)	35.9 kg
Wetted Surface Area (S)	0.71 m^2

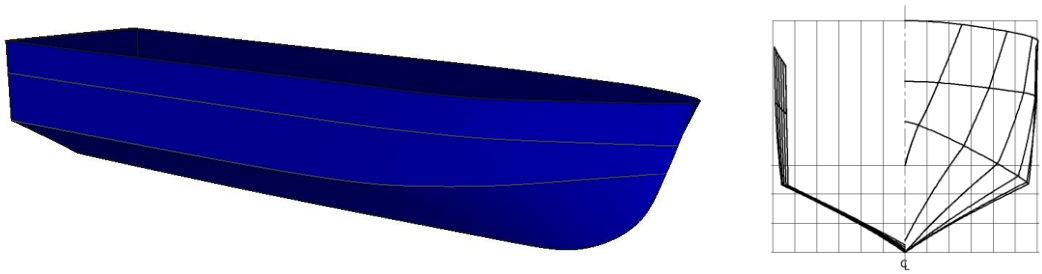

(a) (b)

Fig. 1. Semi-planing monohull hullform (a) 3-Dimension (b) Body plan

In this study, the resistance of different two case conditions were investigated i.e. fixed conditions (without considering trim and sinkage) and free conditions (with considering trim and sinkage). Six

different speeds at Froude numbers, Fr, ranging from 0.2 to 0.7 with increments of 0.1 were simulated.

2.2 Resistance Representation

The resistance was presented in the total resistance (R_T) obtained from the simulation, friction resistance (R_F) calculated based on Eq. (1) and Eq. (2), and residuary resistance (R_R) calculated based on Eq. (3).

$$R_F = 0.5\,\rho\,V^2 S\,C_F \tag{1}$$

$$C_F = \frac{0.075}{(\log_{10} R_e - 2)^2} \tag{2}$$

$$R_R = R_T - R_F \tag{3}$$

where R_T is total resistance, ρ is water density, V is ship speed, S is wetted surface area, C_F is friction resistance coefficient, which is calculated from ITTC 1957 correlation line Eq. (2), and R_e is Reynolds number.

2.3 Numerical Investigation

In this study, a numerical investigation was conducted using ANSYS CFX, which is a commercial CFD software that had been utilized by multiple authors for marine vehicle applications [12-17].

2.3.1 Governing equations and numerical modeling

A three-dimensional CFD model with a Reynolds-averaged Navier-Stokes (RANS) approach to solve flow issues in the walls of ships. They employed the ANSYS-CFX program which was designed specifically for this purpose and employs the constant viscous incompressible flow equation. The two equations, averaged continuity, and momentum equations were used to express incompressible flows in this study [18]. The equations for mass and momentum are presented as Eq. (4) and Eq. (5), respectively.

$$\frac{\partial \rho}{\partial t} + \nabla.(\rho U) = 0 \tag{4}$$

$$\frac{\partial (\rho U)}{\partial t} + \nabla.(\rho U\ x\ U) = -\nabla p + \nabla.\tau + S_M \tag{5}$$

where the stress tensor, τ is related to the strain rate.

The governing equation of total energy is presented in the Eq. (6):

$$\frac{\partial (\rho h_{tot})}{\partial t} - \frac{\partial p}{\partial t} + \nabla.(\rho U h_{tot}) = \nabla(\lambda \nabla T) + \nabla(U.\tau) + U.S_M + S_E \tag{6}$$

where h_{tot} is the total enthalpy.

The expression $+\nabla(U.\tau)$ accounts for the work resulting from viscous stresses and is referred to as the viscous work term. The term $U.S_M$ represents the work resulting from external momentum sources and is presently not taken into consideration.

Additionally, Reynolds-Averaged Navier-Stokes (RANS) was formulated as a modification of the steady Navier-Stokes equations, incorporating both averaged and fluctuating variables. Anderson categorizes the turbulence model based on RANS equations as a statistical turbulence model because it relies on statistical averaging techniques in the derivation of the equations [19].

The SST model effectively formulates a versatile approach for various applications by integrating the advantages of the k-ω model with other relevant factors. To achieve this, it incorporates a blending function called F1, which takes a value of one in the region immediately adjacent to the solid surface and gradually decreases to zero as one moves further away from the wall into the flow domain. This arrangement activates the k-ω model near the wall and employs the k-ε model for the rest of the flow. This approach enables the beneficial near-wall characteristics of the k-ω model to be utilized without the risk of introducing inaccuracies stemming from the model's sensitivity to free stream conditions. The modelled equations for turbulent kinetic energy (k) and turbulence frequency (ω) are shown in Eq. (7) and Eq. (8).

$$\frac{\partial(\rho k)}{\partial t}+\frac{\partial(\partial u_j k)}{\partial x_j}=P-\beta^*\rho\omega k+\frac{\partial}{\partial x_j}\left[(\mu+\sigma_k\mu_t)\frac{\partial k}{\partial x_j}\right] \tag{7}$$

$$\frac{\partial(\rho\omega)}{\partial t}+\frac{\partial(\rho u_j\omega)}{\partial x_j}=\frac{\gamma}{v_t}P-\beta\rho\omega^2+\frac{\partial}{\partial x_j}\left[(\mu+\sigma_\omega\mu_t)\frac{\partial\omega}{\partial x_j}\right]+2(1-F_1)2\rho\sigma_{\omega 2}\frac{1}{\omega}\frac{\partial k}{\partial x_j}\frac{\partial\omega}{\partial x_j} \tag{8}$$

Menter and Esch [20] documented its performance, while a recent NASA Technical Memorandum by Bardina *et al.,* ranked the SST model as the most precise model in its category [21].

In addition to these equations, the dynamic model also included equations of motion for the body, which consider the motion and rotation of the body in six degrees of freedom (DOF). The equation of motion for a rotating rigid body can be rewritten in body-fixed coordinates (about the center of mass) as:

$$\dot{\theta}\times\dot{\theta}+I\ddot{\theta}=m \tag{9}$$

$$I=\begin{bmatrix}\int((y-y_G)^2+(z-z_G)^2)dm & -\int(x-x_G)(y-y_G)dm & -\int(x-x_G)(z-z_G)dm\\ -\int(x-x_G)(y-y_G)dm & \int((x-x_G)^2+(z-z_G)^2)dm & -\int(y-y_G)(z-z_G)dm\\ -\int(x-x_G)(z-z_G)dm & -\int(y-y_G)(z-z_G)dm & \int((x-x_G)^2+(y-y_G)^2)dm\end{bmatrix} \tag{10}$$

In the mass moment of inertia matrix shown in Eq. (9), the center of mass is given by (x_G, y_G,z_G), and is a differential element of mass. Eq. (10) represents the spatial coordinate form for the classical Euler's equation for the rigid body in body-fixed coordinates. Also, in Eq. (11) is the total moment from all the separate contributions including spring and other external moment:

$$m=m_{Aero}-k_{Rotate}(\theta-\theta_{so})+m_{Ext} \tag{11}$$

where m_{Aero} is the aerodynamic torque, k_{Rotate} is the rotational spring constant and m_{Ext} is all other external torques acting on the body.

For wave generation, the Volume of Fluid (VoF) model has been used. In terms of simulations, the waves generated by differentiating between water and air. This is accomplished by assigning a numerical value of 1 to water and 0 to air, effectively establishing the free surface. The existence of

waves is attributed to the fluctuating water fraction, which can range from 0 to 1, and has an impact on the overall dynamics of the simulation. While the relationship between pressure and velocity field has been achieved by using the Rhie-Chow algorithm.

In this study, a steady for fixed condition case and an unsteady for free condition case. Regarding the convective term and the temporal terms, for fixed condition case, the convective term has been discretized by using second order upwind, while the temporal term has not discretized since it used an unsteady simulation. For free condition case, the convective term has been discretized by using second order upwind, while the temporal term by using second order backward Euler.

2.3.2 Boundary condition

The size of the computational domain, as illustrated in Figure 2, was determined based on the total length of the model, which was represented by the variable L. The inlet was positioned at one and a half times the length of the model in front of the model. Similarly, the bottom boundary was set at one and a half times the length of the model from waterline. The top boundary was set at one time the length of the model from waterline. The sides boundaries were set one and a half times the length of the model from center line. Whereas the outlet was located five times the length behind the model.

Furthermore, two boundary conditions were used, one for fixed condition and another for free condition body through the restriction of motion to heave and pitch. Generally, the specified boundary conditions include the following: The top, side, and bottom walls were governed by the free-slip condition. For free condition, the domain of motion and rotation was added. The domain is shown in Figure 2.

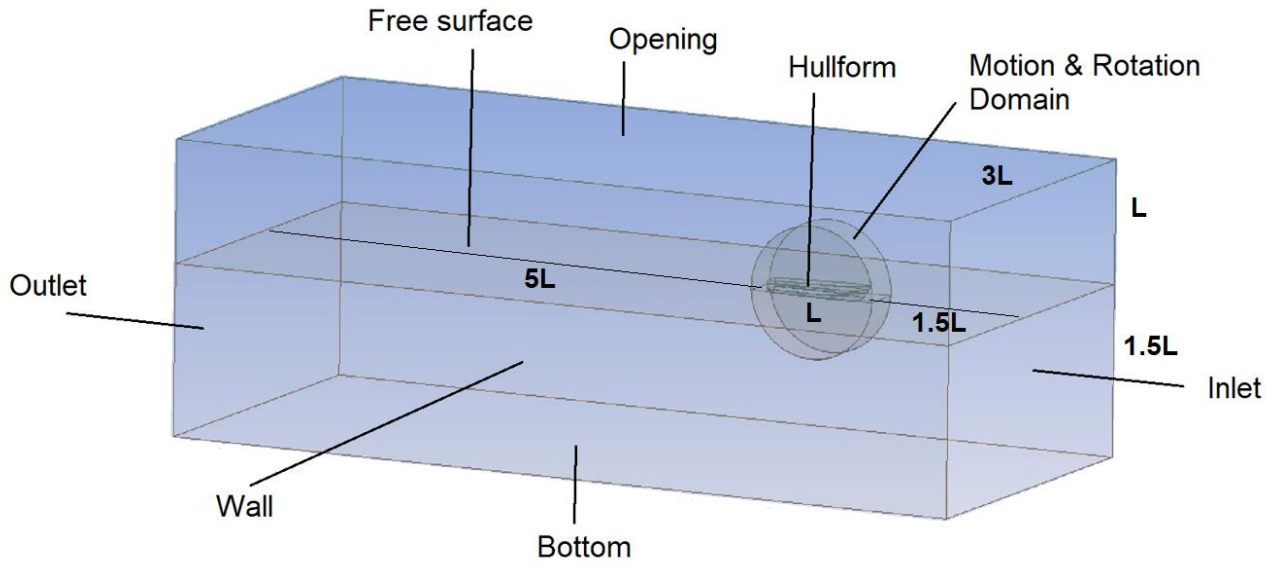

Fig. 2. Boundary conditions

The inlet was set with a flow velocity corresponding to the investigated speed, and at the outlet, the static pressure was imposed as a function of the water-level height. Furthermore, the common definition of the free surface was established by determining the volume-fraction function for water and an equation for the initial water level height.

2.3.3 Grid generation

In this study, the mesh was generated using Design Modeler. To discretize the computational domain, both structured and unstructured meshes were employed. Given the complex geometric characteristics of the hull, a triangular element mesh was created on its surface and further refined the boundary layer using prism elements by expanding the surface mesh nodes. Near the hull, hexahedral components were added to occupy the space, while in the distant field, hybrid mesh with modelling was employed to oversee the effects of flow phenomena surrounding the model hull, it is necessary to implement measures aimed at achieving a smoother flow. Both models employ identical mesh types. In the fixed (Figure 3(a)) general meshing model, the gradient gradually diminishes as it makes contact with the ship model. Whereas the free model (Figure 3(b)) employs a universal meshing approach that is applied outside the sub-domain and gradually diminishes within the sub-domain till it achieves the model.

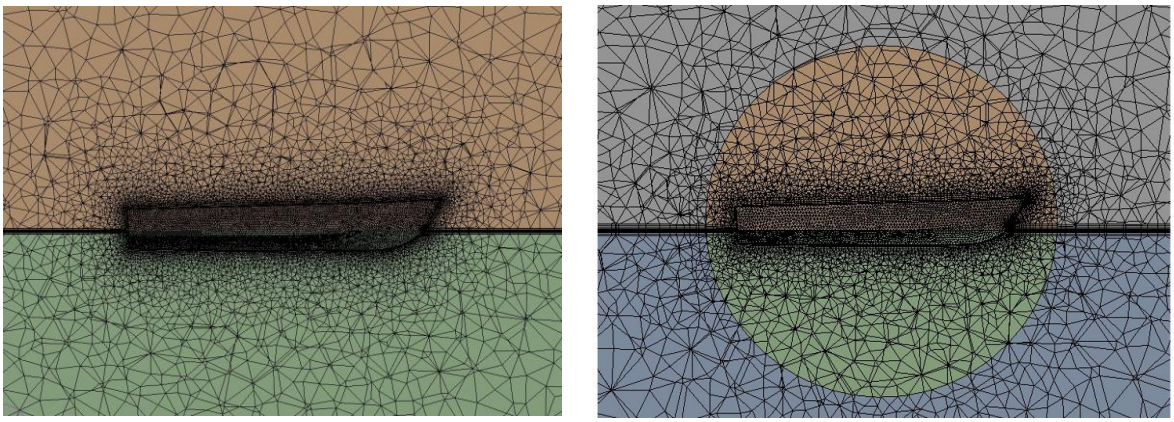

(a) (b)

Fig. 3. Unstructured mesh with inflation (a) fixed (b) free

Selecting an appropriate mesh size was essential for the computational process, as a finer mesh can yield credible results in ANSYS CFX, but it also substantially escalates computational expenses and time requirements. To determine a mesh size, a grid independence study was conducted at Fr 0.2 as the same as in the previous study [11]. The results of grid independence study are shown in Table 2 dan Figure 4.

Table 2
Grid independence study

No.	Element numbers (NE)	C_T
1 (Finest)	3,136,568	0.0111
2	1,402,364	0.0113
3	750,625	0.0122
4	365,564	0.0141
5	170,654	0.0157
6	80,569	0.0197

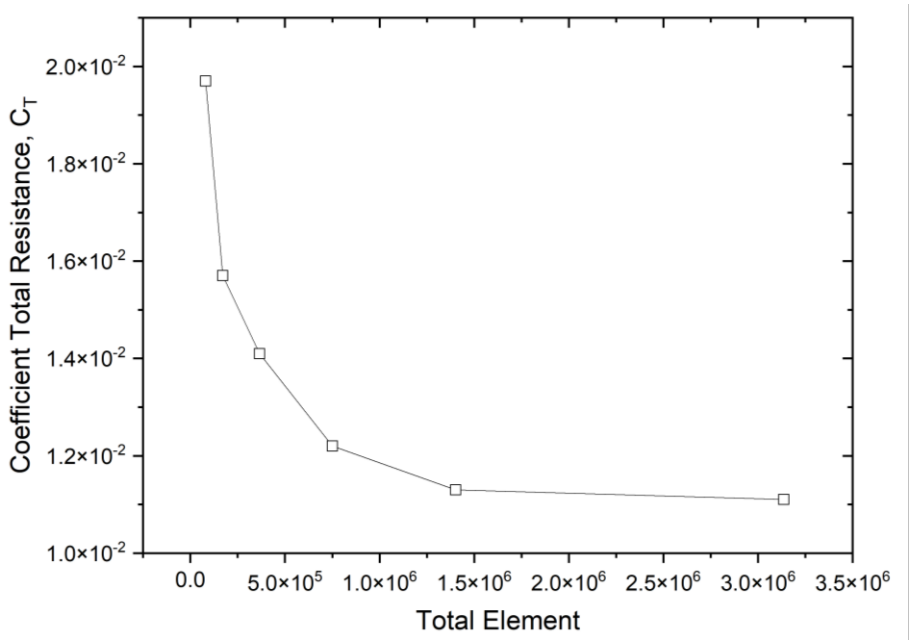

Fig. 4. Grid independence

Grid generation, especially around hull plays a very important role for obtaining accurate flow phenomenon within the boundary layer which is represented by y+ value. In this study, the set up of automatic wall function in ANSYS-CFX was chosen. This allows the software to evaluate y+ and adjust the appropriate wall function.

2.3.4 Verification and validation study

In this study, verification was conducted only for grid convergence study. The study analyzed the uncertainty of the simulation results which represented as Grid convergence index (GCI). The resumed of its uncertainty analysis is presented on Table 3.

Table 3
The uncertainty analysis

Outcome	Equation	Value
Difference of estimation	$\varepsilon_{21}= C_{T2} - C_{T1}$	0.0002
	$\varepsilon_{32}= C_{T3} - C_{T2}$	0.0009
Refinement ratio	$r_i= (NE_2/NE_1)^{1/3} = (NE_3/NE_2)^{1/3}$	1.3
Convergence ratio	$R_i=\varepsilon_{21}/\varepsilon_{32}$	0.22
Order of accuracy	$p=\ln(\varepsilon_{21}/\varepsilon_{32})/\ln(r_i)$	5.61
Extrapolated relative error	$e_{21}= \varepsilon_{21}/(r_i^p-1)$	0.000057
	$e_{32}= \varepsilon_{32}/(r_i^p-1)$	0.000406
Grid convergence index (GCI)	$GCI_{21}=(Fs\|e_{21}\|/ C_{T1}) \times 100\%$	0.6%
	$GCI_{32}= (Fs\|e_{32}\|/ C_{T2}) \times 100\%$	2.8%

From those analysis known that the convergence ratio (R_i) is about 0.22 which means that the convergence condition is monotonic convergence ($0 < Ri < 1$). Therefore, a generalized Richardson extrapolation is applied to estimate the errors and uncertainties. In this calculation, GCI was calculated using safety factor (Fs) of about 1.25.

3. Results and Discussions

The trim and sinkage results are presented in Table 4 and illustrated in Figure 5. It provides a clear visual representation of the trim and sinkage characteristics of the semi-planing monohull model under different flow conditions. These findings highlight the importance of considering the Froude number when analyzing the behavior of such models, as it directly influences their trim and sinkage characteristics.

The findings indicate that at low Froude number, for this case up to Fr 0.4, the model does not exhibit trim. A similar trend also happens at study by Avci and Baris [22]. At Fr 0.5, the trim measured 97 mm by stern, indicating a slight inclination of the vessel. This bow inclination became more pronounced at Fr 0.6, with a trim by stern of 103 mm. Finally, at Fr 0.7, the trim increased further to 108 mm. These findings suggest that as the flow velocity increases, the model undergoes a significant change in its trim characteristics.

In addition to trim, the results indicate that the model did not experience any sinkage at low Froude number, for this case up to Fr 0.3. However, at Fr 0.4, sinkage began to occur, measuring 4 mm. As the Fr increased to 0.5 and 0.6, the sinkage increased to 7 mm and 8 mm, respectively. Interestingly, at Fr 0.7, the model experienced a rise of 4 mm, indicating a deviation from the sinkage trend observed at lower Fr. This phenomenon also happens at study by Avci and Baris [22].

Table 4
Trim and sinkage

Fr	Trim (mm)	Sinkage (mm)
0.2	0	0
0.3	0	0
0.4	0	4
0.5	97	7
0.6	103	8
0.7	108	-4

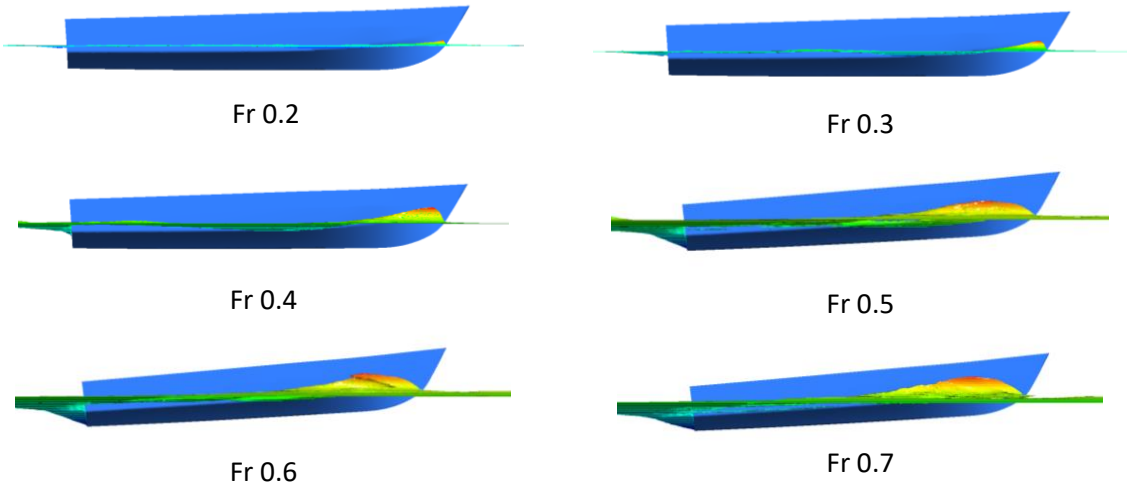

Fig. 5. Trim condition at Fr 0.2 to Fr 0.7

Meanwhile, in light of the aforementioned trim and sinkage conditions, it is observed that the model generates the smallest total resistance, R_T, at 3.07 N. This minimal resistance is achieved at a Fr 0.2. Conversely, the largest R_T 44.12 N is recorded at a Fr 0.7. Comparatively, when analyzing the total resistance results of a ship model that remains fixed without experiencing trim and sinkage, it

becomes apparent that the resistance values are greater by a range of 5.2% to 68.4%. This disparity is clearly illustrated in Table 5 and Figure 6. This presentation highlights the significant impact of trim and sinkage on the total resistance encountered by the model. By varying the Fr value, it is evident that the resistance values fluctuate considerably, with the lowest resistance occurring at Fr 0.2 and the highest at Fr 0.7.

Table 5
Total Resistance, R_T (N)

Fr	Fixed	Free	Discrepancy (%)
0.2	3.1	3.1	0.0
0.3	7.3	7.3	0.0
0.4	14.3	15.0	5.2
0.5	26.3	38.8	47.6
0.6	24.7	41.6	68.4
0.7	30.6	44.1	44.1

To gain a comprehensive understanding of the factors contributing to this deviation, it is crucial to analyze the calculations pertaining to friction resistance (R_F) and residuary resistance (R_R). These two components collectively constitute the total resistance, R_T.

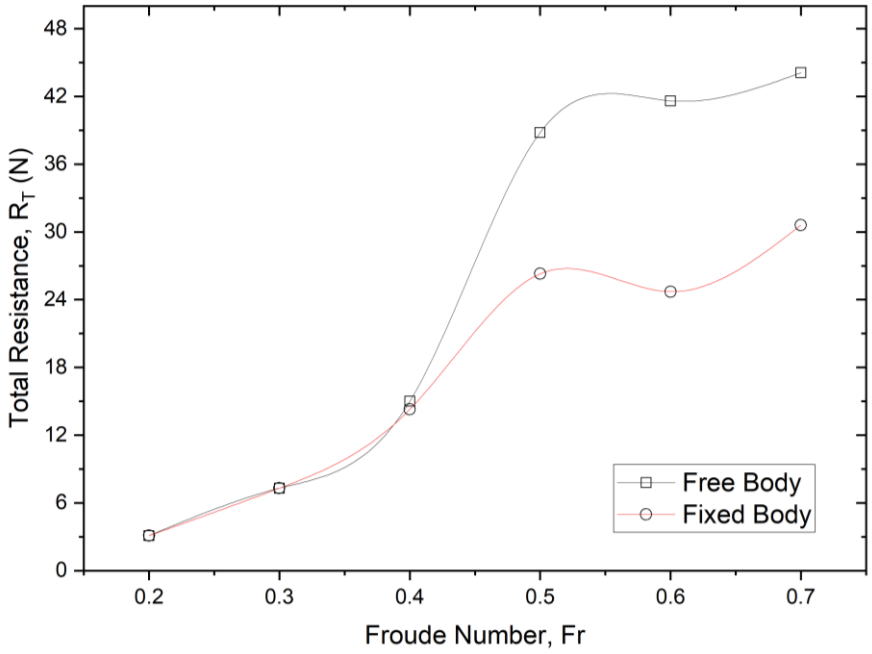

Fig. 6. Total resistance comparison of free (trim-sinkage) and fixed (no trim-sinkage) conditions

Friction resistance plays a crucial role in various fields, and its calculation is based on the equations denoted as Eq. (1) and Eq. (2). One of the key factors that significantly influences friction resistance is the wetted surface area, denoted as S. In most cases, when conditions are fixed, the wetted surface area is assumed to remain constant. However, it is important to note that under certain conditions, such as trim and sinkage, the wetted surface area can undergo changes. These conditions, referred to as free conditions, can lead to variations in the wetted surface area. To better understand the impact of these changes, a comparison between the wetted surface area under fixed and free conditions is presented in Table 6. Upon analyzing Table 6, it becomes evident that the highest difference in wetted surface area is observed at Fr 0.5, with a difference of 7.3%. This finding

highlights the significance of considering the effect of free conditions on the wetted surface area when calculating friction resistance.

The findings of the friction resistance calculation, R_F, are presented in Table 7 and Figure 7. Upon reviewing Table 7, it becomes apparent that the most notable variation in friction resistance between free and fixed conditions amounts to 7.13%, arising at Fr 0.5. This observation implies that the trim and sinkage characteristics of the vessel do not exert a substantial influence on friction resistance.

Table 6
Wetted Surface Area, S (m^2)

Fr	Fixed	Free	Discrepancy (%)
0.2	0.712	0.712	0.0
0.3	0.712	0.712	0.0
0.4	0.712	0.714	0.3
0.5	0.712	0.764	7.3
0.6	0.712	0.759	6.6
0.7	0.712	0.715	0.4

Table 7
Friction Resistance, R_F (N)

Fr	Fixed	Free	Discrepancy (%)
0.2	0.334	0.334	0.00
0.3	0.788	0.788	0.00
0.4	1.448	1.453	0.35
0.5	2.985	3.198	7.13
0.6	3.418	3.638	6.42
0.7	4.740	4.741	0.03

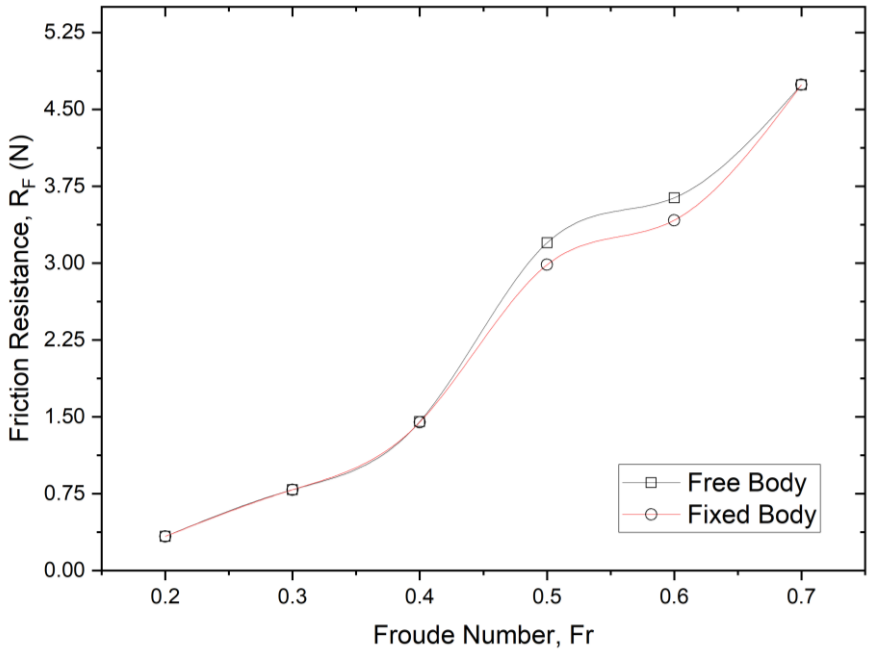

Fig. 7. Friction resistance comparison of fixed and free conditions

Meanwhile, the results of residuary resistance reveal a notable discrepancy between fixed and free conditions. The most substantial variation, amounting to approximately 78.41%, is observed at Fr 0.6, as depicted in Table 8 and Figure 8. This discrepancy underscores the significant impact of trim and sinkage conditions on residuary resistance. The alteration in trim and sinkage influences the generation of waves at

both the bow and stern, consequently affecting the magnitude of wave-making resistance. Wave-making resistance constitutes a crucial constituent of residuary resistance.

.

Table 8
Residuary Resistance, R_R (N)

Fr	Fixed	Free	Discrepancy (%)
0.2	2.73	2.73	0.00
0.3	6.51	6.51	0.00
0.4	12.81	13.54	5.72
0.5	23.29	35.59	52.81
0.6	21.27	37.95	78.41
0.7	25.86	39.38	52.26

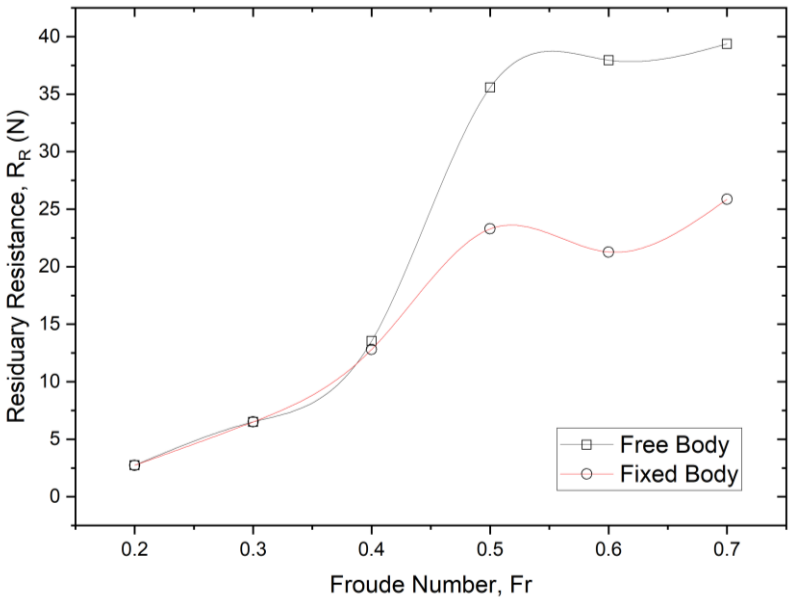

Fig. 8. Residuary resistance comparison of fixed and free conditions

To demonstrate the significant impact of the wave generated by the model on resistance, Figure 9 presents a comparison between the wave contours generated under fixed and free conditions. The figure showcases the different wave patterns at Fr 0.3 to Fr 0.7, with the fixed condition depicted in the upper part and the free condition in the lower part.

Upon analyzing Figure 9, it becomes evident that the waves generated by the model under the free condition are considerably larger when compared to both the fixed and keel conditions. This observation holds true for all three Fr values. The contrasting wave contours depicted in Figure 9 provide compelling evidence for the influence of the model-generated waves on resistance. The significant disparity between the wave patterns under fixed and free conditions suggests that the presence of waves plays a crucial role in determining resistance levels. By presenting this visual comparison, Figure 9 effectively conveys the notion that the wave generated by the model has a substantial impact on resistance. The larger waves observed under the free condition indicate a higher resistance.

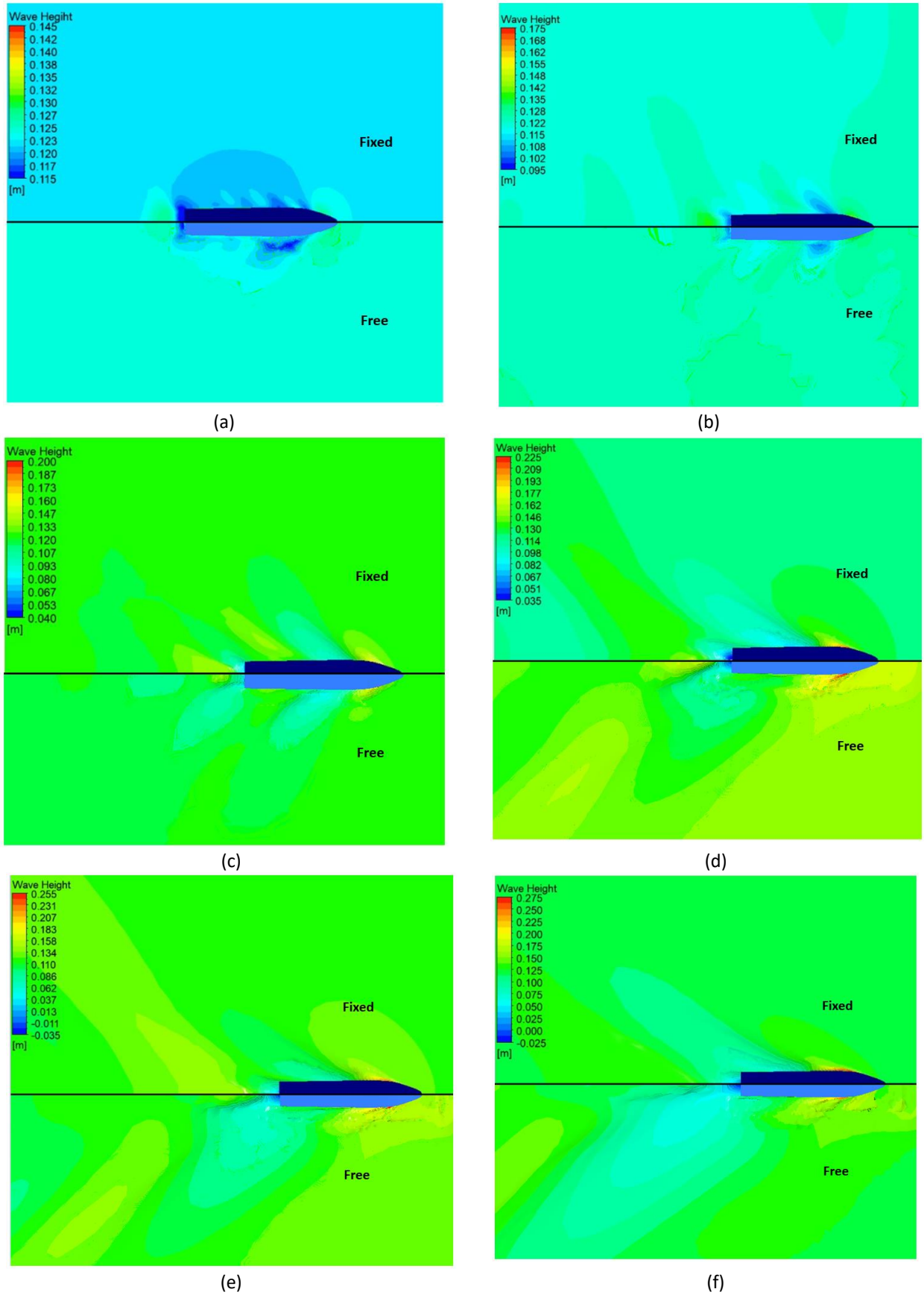

Fig. 9. Wave contour of fixed and free conditions at different Froude numbers (a) Fr 0.2 (b) Fr 0.3 (c) Fr 0.4 (d) Fr 0.5 (e) Fr 0.6 (f) Fr 0.7

This phenomenon poses significant challenges for fast vessels, particularly when trim arises. Consequently, it is crucial to conduct further research in order to mitigate the adverse effects associated with trim, specifically for semi-planing monohulls. From the literature reviews [3-9], the application of stern flaps or stern wedges have shown promising results in mitigating the adverse effects of trim. The use of stern flaps and wedges helps to increase lift on the stern, which in turn reduces the inclination of the hull and improves the total resistance.

4. Conclusions

The investigation of trim and sinkage effects on the resistance of a semi-planing monohull using computational fluid dynamics shows quite satisfactory results. These results can depict the total resistance generated by the model under real conditions (experiencing trim and sinkage) compared to the assumption of the ship not undergoing dynamic movement (fixed). The simulation results reveal that for this model, it experiences trim at a Froude number, Fr 0.5. The trim becomes more significant as Fr increases. As for sinkage, the model already experiences sinkage at Fr 0.4 and continues to increase with higher Fr. However, at Fr 0.7, the model no longer experiences sinkage but instead rises.

As for the model experiencing trim and sinkage, it results in a higher total resistance compared to the fixed condition, with the largest difference being 68.4% occurring at Fr 0.6. The investigation results indicate that the factor influencing the magnitude of total resistance is the residuary resistance, while the friction resistance is not significantly affected by trim and sinkage conditions because, in this case, the changes in wetted surface area are not very significant. As for the factor that influences the magnitude of residuary resistance, it is the wave formation generated by the model experiencing trim and sinkage, which is greater compared to the fixed condition (even keel).

For further study, an investigation by conducting model experiments is suggested to validate the numerical results. Also, an investigation for higher speed at the regime of fully planing is interested to know whether the resistance is lower at this condition compared to fixed condition.

Acknowledgement

The authors wish to thank the ITS Global Engagement, Institut Teknologi Sepuluh Nopember (ITS), for financing the study under the project scheme no. 231/IT2/T/HK.00.01/2023 of World Class Professor (WCP) Program 2023.

References

[1] Riyadi, Soegeng, Wasis Dwi Aryawan, and I. K. A. P. Utama. "Experimental and computational fluid dynamics investigations into the effect of loading condition on resistance of hard-chine semi planning crew boat." *International Journal of Technology* 13, no. 3 (2022): 518-532. https://doi.org/10.14716/ijtech.v13i3.4597

[2] Salas, M., J. Rosas, and R. Luco. "Hydrodynamic analysis of the performance of stern flaps in a semi-displacement hull." *Latin American applied research* 34, no. 4 (2004): 275-284.

[3] Amacher, Robin, Theodora Cohen Liechti, Michael Pfister, Giovanni De Cesare, and Anton J. Schleiss. "Wave-reducing stern flap on ship convoys to protect riverbanks." *Naval Engineers Journal* 127, no. 1 (2015): 95-102.

[4] Cumming, D., R. Pallard, E. Thornhill, D. Hally, and M. Dervin. "Hydrodynamic design of a stern flap appendage for the HALIFAX class frigates." *Mari-Tech, Halifax, NS (June 14-16, 2006)* (2006).

[5] Karafiath, Gabor, Dominic Cusanelli, and Cheng Wen Lin. "Stern wedges and stern flaps for improved powering-US Navy experience." (2011).

[6] Ghassemi, Mohammad A., Parviz Ghadimi, and Sayyed Mahdi Sajedi. "The effect of the stern wedge length and height on the drag and trim of a chine-planing hull." *Zeszyty Naukowe Akademii Morskiej w Szczecinie* 67 (139 (2021): 39-52.

[7] Grigoropoulos, G. J., and T. A. Loukakis. "Effect of wedges on the calm water resistance of planing hulls." In *1st International Conference on Marine Industry, Varna, Bulgaria*. 1996.

[8] Jensen, Niel, and R. Latorre. "Prediction of influence of stern wedges on power boat performance." *Ocean engineering* 19, no. 3 (1992): 303-312. https://doi.org/10.1016/0029-8018(92)90031-X
[9] Karafiath, Gabor. "The effect of stern wedges on ship powering performance." *Naval Engineers Journal* 99, no. 3 (1987): 27-38. https://doi.org/10.1111/j.1559-3584.1987.tb02113.x
[10] Suastika, Ketut, Affan Hidayat, and Soegeng Riyadi. "Effects of the application of a stern foil on ship resistance: A case study of an Orela crew boat." *International Journal of Technology* 8, no. 7 (2017): 1266-1275. https://doi.org/10.14716/ijtech.v8i7.691
[11] Nasirudin, Ahmad, I. Ketut Aria Pria Utama, and Andreas Kukuh Priyasambada. "CFD Analysis into the Resistance Estimation of Hard-Chine Monohull using Conventional against Inverted Bows." *CFD Letters* 15, no. 6 (2023): 54-64. https://doi.org/10.37934/cfdl.15.6.5464
[12] Jabar, Siti Norbakyah, and Salisa Abdul Rahman. "A Comparative Study on Components Sizing for Conventional Boat and Pherb Powertrains using Water Driving Cycle." *Journal of Advanced Research in Applied Sciences and Engineering Technology* 16, no. 1 (2019): 41-48.
[13] Waskito, Kurniawan Teguh. "On the High-Performance Hydrodynamics Design of a Trimaran Fishing Vessel." *Journal of Advanced Research in Fluid Mechanics and Thermal Sciences* 83, no. 1 (2021): 17-33. https://doi.org/10.37934/arfmts.83.1.1733
[14] Utomo, Allessandro Setyo Anggito. "Comparison of Drag Reduction Effect on Barge Model Ship Using Ultrafine Bubble and Microbubble Injection." *Journal of Advanced Research in Fluid Mechanics and Thermal Sciences* 96, no. 2 (2022): 134-143. https://doi.org/10.37934/arfmts.96.2.134143
[15] Utama, I. K. A. P., and I. K. Suastika. "Experimental and Numerical Investigation into the Effect of the Axe-Bow on the Drag Reduction of a Trimaran Configuration." *International Journal of Technology* 12, no. 3 (2021): 527-538. https://doi.org/10.14716/ijtech.v12i3.4659
[16] Sutiyo, I., and I. Ketut Aria Pria Utama. "CFD Analysis into the Drag Characteristics of Trimaran Vessel: Comparative Study between Standard NPL 4a and the use of Axe-Bow." In *IOP Conference Series: Earth and Environmental Science*, vol. 799, no. 1, p. 012007. IOP Publishing, 2021. https://doi.org/10.1088/1755-1315/799/1/012007
[17] Elhadad, Alaaeldeen M., and Abo El-Ela. "Experimental and Cfd Resistance Validation of Naval Combatant Dtmb 5415 Model." *Journal of Advanced Research in Fluid Mechanics and Thermal Sciences* 107, no. 2 (2023): 84-102. https://doi.org/10.37934/arfmts.107.2.84102
[18] Ansys, C. "Ansys Cfx-Solver Modeling Guide. Canonsburg, PA, USA: ANSYS." (2020).
[19] Anderson, John David, and John Wendt. *Computational fluid dynamics*. Vol. 206. New York: McGraw-hill, 1995.
[20] Menter, Florian R. "Elements of inductrial heat tranfer predictions." In *16th Brazilian Congress of Mechanical Engineering (COBEM), Uberlandia, Brazil, 2001*. 2001.
[21] Bardina, J. E. P. G., P. Huang, T. Coakley, J. Bardina, P. Huang, and T. Coakley. "Turbulence modeling validation." In *28th Fluid dynamics conference*, p. 2121. 1997. https://doi.org/10.2514/6.1997-2121
[22] Avci, Ahmet Gültekin, and Barış Barlas. "A practical application for trim and sinkage measurements for high speed marine vessels by using an inertial measurement unit and an arduino board." In *4th international conference on advanced model measurement technology for the maritime industry, Istanbul*. 2015.